

Diffractive Dijet Cross Sections in Photoproduction at HERA

ZEUS Collaboration

Abstract

Differential dijet cross sections have been measured with the ZEUS detector for photoproduction events in which the hadronic final state containing the jets is separated with respect to the outgoing proton direction by a large rapidity gap. The cross section has been measured as a function of the fraction of the photon (x_γ^{OBS}) and pomeron (β^{OBS}) momentum participating in the production of the dijet system. The observed x_γ^{OBS} dependence shows evidence for the presence of a resolved- as well as a direct-photon component. The measured cross section $d\sigma/d\beta^{OBS}$ increases as β^{OBS} increases indicating that there is a sizeable contribution to dijet production from those events in which a large fraction of the pomeron momentum participates in the hard scattering. These cross sections and the ZEUS measurements of the diffractive structure function can be described by calculations based on parton densities in the pomeron which evolve according to the QCD evolution equations and include a substantial hard momentum component of gluons in the pomeron.

The ZEUS Collaboration

J. Breitweg, M. Derrick, D. Krakauer, S. Magill, D. Mikunas, B. Musgrave, J. Repond, R. Stanek,
R.L. Talaga, R. Yoshida, H. Zhang
Argonne National Laboratory, Argonne, IL, USA ^p

M.C.K. Mattingly
Andrews University, Berrien Springs, MI, USA

F. Anselmo, P. Antonioli, G. Bari, M. Basile, L. Bellagamba, D. Boscherini, A. Bruni, G. Bruni,
G. Cara Romeo, G. Castellini¹, L. Cifarelli², F. Cindolo, A. Contin, N. Coppola, M. Corradi,
S. De Pasquale, P. Giusti, G. Iacobucci, G. Laurenti, G. Levi, A. Margotti, T. Massam,
R. Nania, F. Palmonari, A. Pesci, A. Polini, G. Sartorelli, Y. Zamora Garcia³, A. Zichichi
University and INFN Bologna, Bologna, Italy ^f

C. Amelung, A. Bornheim, I. Brock, K. Coböken, J. Crittenden, R. Deffner, M. Eckert,
M. Grothe⁴, H. Hartmann, K. Heinloth, L. Heinz, E. Hilger, H.-P. Jakob, A. Kappes, U.F. Katz,
R. Kerger, E. Paul, M. Pfeiffer, J. Stamm⁵, H. Wieber
Physikalisches Institut der Universität Bonn, Bonn, Germany ^c

D.S. Bailey, S. Campbell-Robson, W.N. Cottingham, B. Foster, R. Hall-Wilton, G.P. Heath,
H.F. Heath, J.D. McFall, D. Piccioni, D.G. Roff, R.J. Tapper
H.H. Wills Physics Laboratory, University of Bristol, Bristol, U.K. ^o

R. Ayad, M. Capua, L. Iannotti, M. Schioppa, G. Susinno
Calabria University, Physics Dept.and INFN, Cosenza, Italy ^f

J.Y. Kim, J.H. Lee, I.T. Lim, M.Y. Pac⁶
Chonnam National University, Kwangju, Korea ^h

A. Caldwell⁷, N. Cartiglia, Z. Jing, W. Liu, B. Mellado, J.A. Parsons, S. Ritz⁸, S. Sampson,
F. Sciulli, P.B. Straub, Q. Zhu
Columbia University, Nevis Labs., Irvington on Hudson, N.Y., USA ^q

P. Borzemeski, J. Chwastowski, A. Eskreys, J. Figiel, K. Klimek, M.B. Przybycień, L. Zawiejski
Inst. of Nuclear Physics, Cracow, Poland ^j

L. Adamczyk⁹, B. Bednarek, M. Bukowy, A.M. Czermak, K. Jeleń, D. Kisielewska,
T. Kowalski, M. Przybycień, E. Rulikowska-Zarębska, L. Suszycki, J. Zajac
Faculty of Physics and Nuclear Techniques, Academy of Mining and Metallurgy, Cracow, Poland ^j

Z. Duliński, A. Kotański
Jagellonian Univ., Dept. of Physics, Cracow, Poland ^k

G. Abbiendi¹⁰, L.A.T. Bauerdick, U. Behrens, H. Beier, J.K. Bienlein, K. Desler, G. Drews,
U. Fricke, I. Gialas¹¹, F. Goebel, P. Göttlicher, R. Graciani, T. Haas, W. Hain, D. Hasell¹²,
K. Hebbel, K.F. Johnson¹³, M. Kasemann, W. Koch, U. Kötz, H. Kowalski, L. Lindemann,
B. Löhr, J. Milewski, M. Milite, T. Monteiro¹⁴, J.S.T. Ng¹⁵, D. Notz, I.H. Park¹⁶, A. Pellegrino,
F. Pelucchi, K. Piotrkowski, M. Rohde, J. Roldán¹⁷, J.J. Ryan¹⁸, A.A. Savin, U. Schneekloth,
O. Schwarzer, F. Selonke, S. Stonjek, B. Surov¹⁹, E. Tassi, D. Westphal, G. Wolf, U. Wollmer,
C. Youngman, W. Zeuner
Deutsches Elektronen-Synchrotron DESY, Hamburg, Germany

B.D. Burow, C. Coldewey, H.J. Grabosch, A. Meyer, S. Schlenstedt
DESY-IfH Zeuthen, Zeuthen, Germany

G. Barbagli, E. Gallo, P. Pelfer
University and INFN, Florence, Italy^f

G. Maccarrone, L. Votano
INFN, Laboratori Nazionali di Frascati, Frascati, Italy^f

A. Bamberger, S. Eisenhardt, P. Markun, H. Raach, T. Trefzger²⁰, S. Wölfle
Fakultät für Physik der Universität Freiburg i.Br., Freiburg i.Br., Germany^c

J.T. Bromley, N.H. Brook, P.J. Bussey, A.T. Doyle²¹, N. Macdonald, D.H. Saxon, L.E. Sinclair,
I.O. Skillicorn, E. Strickland, R. Waugh
Dept. of Physics and Astronomy, University of Glasgow, Glasgow, U.K.^o

I. Bohnet, N. Gendner, U. Holm, A. Meyer-Larsen, H. Salehi, K. Wick
Hamburg University, I. Institute of Exp. Physics, Hamburg, Germany^c

A. Garfagnini, L.K. Gladilin²², D. Horstmann, D. Kçira²³, R. Klanner, E. Lohrmann, G. Poelz,
W. Schott¹⁸, F. Zetsche
Hamburg University, II. Institute of Exp. Physics, Hamburg, Germany^c

T.C. Bacon, I. Butterworth, J.E. Cole, G. Howell, L. Lamberti²⁴, K.R. Long, D.B. Miller,
N. Pavel, A. Priniyas²⁵, J.K. Sedgbeer, D. Sideris, R. Walker
Imperial College London, High Energy Nuclear Physics Group, London, U.K.^o

U. Mallik, S.M. Wang, J.T. Wu
University of Iowa, Physics and Astronomy Dept., Iowa City, USA^p

P. Cloth, D. Filges
Forschungszentrum Jülich, Institut für Kernphysik, Jülich, Germany

J.I. Fleck¹⁹, T. Ishii, M. Kuze, I. Suzuki²⁶, K. Tokushuku, S. Yamada, K. Yamauchi, Y. Yamazaki²⁷
Institute of Particle and Nuclear Studies, KEK, Tsukuba, Japan^g

S.J. Hong, S.B. Lee, S.W. Nam²⁸, S.K. Park
Korea University, Seoul, Korea^h

F. Barreiro, J.P. Fernández, G. García, C. Glasman²⁹, J.M. Hernández, L. Hervás¹⁹, L. Labarga,
M. Martínez, J. del Peso, J. Puga, J. Terrón, J.F. de Trocóniz
Univer. Autónoma Madrid, Depto de Física Teórica, Madrid, Spainⁿ

F. Corriveau, D.S. Hanna, J. Hartmann, L.W. Hung, W.N. Murray, A. Ochs, M. Riveline,
D.G. Stairs, M. St-Laurent, R. Ullmann
McGill University, Dept. of Physics, Montréal, Québec, Canada^{a, b}

T. Tsurugai
Meiji Gakuin University, Faculty of General Education, Yokohama, Japan

V. Bashkirov, B.A. Dolgoshein, A. Stifutkin
Moscow Engineering Physics Institute, Moscow, Russia^l

G.L. Bashindzhagyan, P.F. Ermolov, Yu.A. Golubkov, L.A. Khein, N.A. Korotkova,
I.A. Korzhavina, V.A. Kuzmin, O.Yu. Lukina, A.S. Proskuryakov, L.M. Shcheglova³⁰,
A.N. Solomin³⁰, S.A. Zotkin

Moscow State University, Institute of Nuclear Physics, Moscow, Russia^m

C. Bokel, M. Botje, N. Brümmer, J. Engelen, E. Koffeman, P. Kooijman, A. van Sighem,
H. Tiecke, N. Tuning, W. Verkerke, J. Vosseveld, L. Wiggers, E. de Wolf

NIKHEF and University of Amsterdam, Amsterdam, Netherlandsⁱ

D. Acosta³¹, B. Bylsma, L.S. Durkin, J. Gilmore, C.M. Ginsburg, C.L. Kim, T.Y. Ling,
P. Nylander, T.A. Romanowski³²

Ohio State University, Physics Department, Columbus, Ohio, USA^p

H.E. Blaikley, R.J. Cashmore, A.M. Cooper-Sarkar, R.C.E. Devenish, J.K. Edmonds,
J. Große-Knetter³³, N. Harnew, C. Nath, V.A. Noyes³⁴, A. Quadt, O. Ruske, J.R. Tickner²⁵,
R. Walczak, D.S. Waters

Department of Physics, University of Oxford, Oxford, U.K.^o

A. Bertolin, R. Brugnera, R. Carlin, F. Dal Corso, U. Dosselli, S. Limentani, M. Morandin,
M. Posocco, L. Stanco, R. Stroili, C. Voci

Dipartimento di Fisica dell'Università and INFN, Padova, Italy^f

J. Bulmahn, B.Y. Oh, J.R. Okrasinski, W.S. Toothacker, J.J. Whitmore

Pennsylvania State University, Dept. of Physics, University Park, PA, USA^q

Y. Iga

Polytechnic University, Sagamihara, Japan^g

G. D'Agostini, G. Marini, A. Nigro, M. Raso

Dipartimento di Fisica, Univ. 'La Sapienza' and INFN, Rome, Italy^f

J.C. Hart, N.A. McCubbin, T.P. Shah

Rutherford Appleton Laboratory, Chilton, Didcot, Oxon, U.K.^o

D. Epperson, C. Heusch, J.T. Rahn, H.F.-W. Sadrozinski, A. Seiden, R. Wichmann, D.C. Williams
University of California, Santa Cruz, CA, USA^p

H. Abramowicz³⁵, G. Briskin, S. Dagan³⁶, S. Kananov³⁶, A. Levy³⁶

*Raymond and Beverly Sackler Faculty of Exact Sciences, School of Physics, Tel-Aviv University,
Tel-Aviv, Israel^e*

T. Abe, T. Fusayasu, M. Inuzuka, K. Nagano, K. Umemori, T. Yamashita

Department of Physics, University of Tokyo, Tokyo, Japan^g

R. Hamatsu, T. Hirose, K. Homma³⁷, S. Kitamura³⁸, T. Matsushita

Tokyo Metropolitan University, Dept. of Physics, Tokyo, Japan^g

M. Arneodo, R. Cirio, M. Costa, M.I. Ferrero, S. Maselli, V. Monaco, C. Peroni, M.C. Petrucci,
M. Ruspa, R. Sacchi, A. Solano, A. Staiano

Università di Torino, Dipartimento di Fisica Sperimentale and INFN, Torino, Italy^f

M. Dardo

II Faculty of Sciences, Torino University and INFN - Alessandria, Italy^f

D.C. Bailey, C.-P. Fagerstroem, R. Galea, G.F. Hartner, K.K. Joo, G.M. Levman, J.F. Martin, R.S. Orr, S. Polenz, A. Sabetfakhri, D. Simmons, R.J. Teuscher¹⁹
University of Toronto, Dept. of Physics, Toronto, Ont., Canada^a

J.M. Butterworth, C.D. Catterall, M.E. Hayes, T.W. Jones, J.B. Lane, R.L. Saunders, M.R. Sutton, M. Wing
University College London, Physics and Astronomy Dept., London, U.K.^o

J. Ciborowski, G. Grzelak³⁹, M. Kasprzak, R.J. Nowak, J.M. Pawlak, R. Pawlak, T. Tymieniecka, A.K. Wróblewski, J.A. Zakrzewski, A.F. Żarnecki
Warsaw University, Institute of Experimental Physics, Warsaw, Poland^j

M. Adamus
Institute for Nuclear Studies, Warsaw, Poland^j

O. Deppe, Y. Eisenberg³⁶, D. Hochman, U. Karshon³⁶
Weizmann Institute, Department of Particle Physics, Rehovot, Israel^d

W.F. Badgett, D. Chapin, R. Cross, S. Dasu, C. Foudas, R.J. Loveless, S. Mattingly, D.D. Reeder, W.H. Smith, A. Vaiciulis, M. Wodarczyk
University of Wisconsin, Dept. of Physics, Madison, WI, USA^p

A. Deshpande, S. Dhawan, V.W. Hughes
Yale University, Department of Physics, New Haven, CT, USA^p

S. Bhadra, W.R. Frisken, M. Khakzad, W.B. Schmidke
York University, Dept. of Physics, North York, Ont., Canada^a

¹ also at IROE Florence, Italy
² now at Univ. of Salerno and INFN Napoli, Italy
³ supported by Worldlab, Lausanne, Switzerland
⁴ now at University of California, Santa Cruz, USA
⁵ now at C. Plath GmbH, Hamburg
⁶ now at Dongshin University, Naju, Korea
⁷ also at DESY
⁸ Alfred P. Sloan Foundation Fellow
⁹ supported by the Polish State Committee for Scientific Research, grant No. 2P03B14912
¹⁰ now at INFN Bologna
¹¹ now at Univ. of Crete, Greece
¹² now at Massachusetts Institute of Technology, Cambridge, MA, USA
¹³ visitor from Florida State University
¹⁴ supported by European Community Program PRAXIS XXI
¹⁵ now at DESY-Group FDET
¹⁶ visitor from Kyungpook National University, Taegu, Korea, partially supported by DESY
¹⁷ now at IFIC, Valencia, Spain
¹⁸ now a self-employed consultant
¹⁹ now at CERN
²⁰ now at ATLAS Collaboration, Univ. of Munich
²¹ also at DESY and Alexander von Humboldt Fellow at University of Hamburg
²² on leave from MSU, supported by the GIF, contract I-0444-176.07/95
²³ supported by DAAD, Bonn
²⁴ supported by an EC fellowship
²⁵ PPARC Post-doctoral Fellow
²⁶ now at Osaka Univ., Osaka, Japan
²⁷ supported by JSPS Postdoctoral Fellowships for Research Abroad
²⁸ now at Wayne State University, Detroit
²⁹ supported by an EC fellowship number ERBFMBICT 972523
³⁰ partially supported by the Foundation for German-Russian Collaboration DFG-RFBR
(grant no. 436 RUS 113/248/3 and no. 436 RUS 113/248/2)
³¹ now at University of Florida, Gainesville, FL, USA
³² now at Department of Energy, Washington
³³ supported by the Feodor Lynen Program of the Alexander von Humboldt foundation
³⁴ Glasstone Fellow
³⁵ an Alexander von Humboldt Fellow at University of Hamburg
³⁶ supported by a MINERVA Fellowship
³⁷ now at ICEPP, Univ. of Tokyo, Tokyo, Japan
³⁸ present address: Tokyo Metropolitan College of Allied Medical Sciences, Tokyo 116, Japan
³⁹ supported by the Polish State Committee for Scientific Research, grant No. 2P03B09308

- a* supported by the Natural Sciences and Engineering Research Council of Canada (NSERC)
- b* supported by the FCAR of Québec, Canada
- c* supported by the German Federal Ministry for Education and Science, Research and Technology (BMBF), under contract numbers 057BN19P, 057FR19P, 057HH19P, 057HH29P
- d* supported by the MINERVA Gesellschaft für Forschung GmbH, the German Israeli Foundation, the U.S.-Israel Binational Science Foundation, and by the Israel Ministry of Science
- e* supported by the German-Israeli Foundation, the Israel Science Foundation, the U.S.-Israel Binational Science Foundation, and by the Israel Ministry of Science
- f* supported by the Italian National Institute for Nuclear Physics (INFN)
- g* supported by the Japanese Ministry of Education, Science and Culture (the Monbusho) and its grants for Scientific Research
- h* supported by the Korean Ministry of Education and Korea Science and Engineering Foundation
- i* supported by the Netherlands Foundation for Research on Matter (FOM)
- j* supported by the Polish State Committee for Scientific Research, grant No. 115/E-343/SPUB/P03/002/97, 2P03B10512, 2P03B10612, 2P03B14212, 2P03B10412
- k* supported by the Polish State Committee for Scientific Research (grant No. 2P03B08308) and Foundation for Polish-German Collaboration
- l* partially supported by the German Federal Ministry for Education and Science, Research and Technology (BMBF)
- m* supported by the Fund for Fundamental Research of Russian Ministry for Science and Education and by the German Federal Ministry for Education and Science, Research and Technology (BMBF)
- n* supported by the Spanish Ministry of Education and Science through funds provided by CICYT
- o* supported by the Particle Physics and Astronomy Research Council
- p* supported by the US Department of Energy
- q* supported by the US National Science Foundation

1 Introduction

A successful phenomenological description of the available data on soft diffractive processes has been obtained using Regge theory and the exchange of a trajectory with the quantum numbers of the vacuum, the pomeron (\mathbb{P}). Hard processes in diffractive reactions [1, 2, 3, 4, 5, 6, 7, 8] provide a tool to investigate the partonic nature of this colour-singlet exchange and to test the universality of its properties in different reactions.

The first experimental evidence pointing to a partonic nature of the pomeron was the observation of jet production in $\bar{p}p$ collisions with a tagged leading proton (or antiproton) made by the UA8 Collaboration [9] following the proposal of Ingelman and Schlein [1]. At HERA, the ZEUS and H1 Collaborations observed neutral-current deep-inelastic ep scattering (DIS) events at high Q^2 (where Q^2 is the virtuality of the exchanged photon) characterised by a large rapidity gap from the proton direction [10, 11]. The properties of these events were suggestive of a diffractive interaction mediated by pomeron exchange between a highly-virtual photon and a proton. The observed Q^2 dependence indicated a pointlike nature of the interaction and a leading-twist mechanism. Measurements of the diffractive structure function in DIS [12, 13, 14] were found to be consistent within the experimental uncertainties with a diffractive structure function which factorises into a pomeron flux factor, which depends on the momentum fraction lost by the proton (x_P), and a pomeron structure function, which depends on Q^2 and the momentum fraction of the struck quark within the pomeron (β). The pomeron structure function showed an approximate scaling with Q^2 at fixed β . More recent H1 measurements [15] have been analysed in terms of parton densities in the pomeron which evolve according to the DGLAP equations [16]. The observed scaling violations indicate that most of the momentum of the pomeron is carried by gluons.

Diffractive photoproduction ($Q^2 \approx 0$) of high transverse energy jets at HERA provides a process which is sensitive both to the quark (e.g. via $\gamma q \rightarrow qg$) and gluon (e.g. via $\gamma g \rightarrow q\bar{q}$) densities in the pomeron. The results on the diffractive structure function in DIS [13], combined with the measured inclusive jet cross sections in diffractive photoproduction gave the first experimental evidence for a gluon content of the pomeron [17]. The data indicated that between 30% and 80% of the momentum of the pomeron carried by partons is due to hard gluons. The conclusion was based on the assumption that the same pomeron flux factor (“Regge factorisation”) and the same pomeron parton densities apply to diffractive DIS and to diffractive jet photoproduction at similar hard scales (“hard-scattering factorisation”).

The CDF Collaboration has recently observed diffractive production of both W -bosons [18] and dijet events [19] in $\bar{p}p$ collisions at $\sqrt{s} = 1.8$ TeV. The analysis of these measurements yields an estimate of the hard-gluon content of the pomeron of $(70 \pm 20)\%$ [19], which is in agreement with the result obtained at HERA [15, 17]. However, the fraction of the total pomeron momentum carried by partons, assuming the pomeron flux factor of Donnachie and Landshoff [3], is well below our result [17]. This discrepancy could be an indication of a breakdown of hard-scattering factorisation for diffractive hard processes in $\bar{p}p$ interactions [19, 20, 21].

Diffractive photoproduction of dijets is sensitive to the underlying two-body processes. In leading-order (LO) QCD two types of processes contribute to jet production [22, 23]: either the photon interacts directly with a parton in the pomeron (the *direct* process) or the photon acts as a source of partons which scatter off those in the pomeron (the *resolved* process). Examples of Feynman diagrams for diffractive dijet photoproduction are shown in Figure 1. The cross section dependence on the fraction of the photon momentum participating in the production of the two jets, x_γ^{OBS} , is sensitive to the presence of these two components [24, 25].

In this paper, new measurements of differential cross sections for diffractive dijet photoproduction at HERA are presented. The results are presented as a function of the pseudorapidity¹ (η^{jet}) and transverse energy of each jet (E_T^{jet}), the γp centre-of-mass energy (W), x_γ^{OBS} and the fraction of the pomeron momentum (β^{OBS}) participating in the production of the two jets with highest E_T^{jet} in an event. These measurements together with those of the diffractive structure function [13] are analysed in terms of parton densities in the pomeron which are assumed to evolve according to the DGLAP equations. We therefore test whether it is possible to describe both sets of data with the same pomeron parton densities, assuming Regge factorisation. The data sample used in this analysis was collected with the ZEUS detector in e^+p interactions at the HERA collider and corresponds to an integrated luminosity of 2.65 pb^{-1} .

2 Kinematics of diffractive hard processes

Diffractive photon-dissociative processes² in e^+p collisions are characterised by a final state consisting of a hadronic system X, the scattered positron and the scattered proton

$$e^+(k) + p_i(P) \rightarrow e^+(k') + X + p_f(P'),$$

where p_i (p_f) denotes the initial (final) state proton. The kinematics of this process are described in terms of four variables. Two of them describe the positron-photon vertex and can be taken to be the virtuality of the exchanged photon (Q^2) and the inelasticity variable y defined by

$$Q^2 = -q^2 = -(k - k')^2 \quad \text{and} \quad y = \frac{P \cdot q}{P \cdot k}.$$

The other two variables describe the proton vertex: the fraction of the momentum of the initial proton carried by the pomeron (x_P), and the square of the momentum transfer (t) between the initial and final state proton, defined by

$$x_P = \frac{(P - P') \cdot q}{P \cdot q} \quad \text{and} \quad t = (P - P')^2.$$

The hard scale is given by Q in diffractive DIS and by the jet transverse energy in diffractive photoproduction ($Q^2 \approx 0$). In DIS, an additional and useful kinematic variable is given by

$$\beta = \frac{Q^2}{2(P - P') \cdot q} = \frac{Q^2}{s y x_P},$$

where \sqrt{s} is the e^+p centre-of-mass energy. In models where the pomeron has a partonic structure, β is the equivalent of the Bjorken- x variable in e^+P interactions.

In diffractive dijet photoproduction processes the hadronic system X contains at least two jets,

$$e^+(k) + p_i(P) \rightarrow e^+(k') + X + p_f(P') \rightarrow e^+(k') + X(\text{jet} + \text{jet} + X_r) + p_f(P'), \quad (1)$$

¹The ZEUS coordinate system is defined as right-handed with the Z axis pointing in the proton beam direction, hereafter referred to as forward, and the X axis horizontal, pointing towards the centre of HERA. The pseudorapidity is defined as $\eta = -\ln(\tan \frac{\theta}{2})$, where the polar angle θ is taken with respect to the proton beam direction.

²These processes will be henceforth referred to as diffractive processes unless otherwise stated.

where X_r denotes the remainder of the final state X not assigned to the two jets with the highest E_T^{jet} . In two-to-two massless-parton scattering, the fractions of the photon (x_γ) and pomeron (β_P) momenta carried by the initial-state partons (in the infinite-momentum frame of the parent particles) are defined by

$$x_\gamma = \frac{(p_{J1} + p_{J2}) \cdot q'}{q \cdot q'} \quad \text{and} \quad \beta_P = \frac{(p_{J1} + p_{J2}) \cdot q}{q \cdot q'},$$

where p_{J1} and p_{J2} are the momenta of the two final state partons, q' is defined as $q' \equiv P - P'$ and the approximations $q^2 \approx q'^2 \approx 0$ have been used. For LO direct processes, $x_\gamma = 1$.

Since the partons are not measurable objects, the observables x_γ^{OBS} [25] and β^{OBS} , defined in terms of jets, are introduced,

$$x_\gamma^{OBS} = \frac{\sum_{jets} E_T^{jet} e^{-\eta^{jet}}}{2y E_e} \quad \text{and} \quad \beta^{OBS} = \frac{\sum_{jets} E_T^{jet} e^{\eta^{jet}}}{2x_P E_p},$$

where E_e (E_p) is the incident positron (proton) energy and the sum runs over the two jets of highest E_T^{jet} in an event. The variable x_γ^{OBS} (β^{OBS}) is an estimator of the fraction of the photon (pomeron) momentum participating in the production of the two jets with highest E_T^{jet} . The LO direct and resolved processes populate different regions of x_γ^{OBS} , with the direct processes being concentrated at high values of x_γ^{OBS} .

Diffractive processes give rise to a large rapidity gap between the hadronic system X and the scattered proton: $\Delta \mathbf{y}_{GAP} = \mathbf{y}_{p_f} - \mathbf{y}_{max}^{had}$, where \mathbf{y}_{p_f} is the rapidity of the scattered proton and \mathbf{y}_{max}^{had} is the rapidity of the most-forward-going hadron belonging to the system X . Instead of \mathbf{y}_{max}^{had} the pseudorapidity (η_{max}^{had}) of the most-forward-going hadron in the detector was used to select diffractive events. The same signature is expected for double dissociation where the scattered proton is replaced by a low-mass baryonic system (N). In this measurement, the outgoing proton (or system N) was not observed.

3 A model for diffractive hard processes

Several models have been developed to describe diffractive hard processes assuming that the main mechanism for reaction (1) is pomeron emission by the proton. The measurements of the diffractive structure function [13] and of the dijet cross sections in diffractive photoproduction presented here are analysed in terms of a model in which both Regge and hard-scattering factorisation are assumed [1, 2, 3, 4, 8] (factorisable model). In this model, first proposed by Ingelman and Schlein [1], resolved- and direct-photon contributions to dijet diffractive photoproduction can be calculated. Additional coherent-pomeron contributions are expected in resolved photoproduction from processes in which the whole pomeron initiates the hard scattering [5, 7, 6]. In principle such contributions would lead to factorisation breaking. However, the inclusion of a delta-function term at $\beta = 1$ in the gluon density of the pomeron in the factorisable model would lead to a similar β distribution.

In QCD, the factorisation theorem [26] ensures that the parton densities (for a given hadron) extracted from measurements of DIS apply also to other inclusive hard processes involving the same initial-state hadron. This theorem has been recently extended to diffractive DIS [27] which justifies our analysis of the leading-twist diffractive structure function in terms of parton densities in the pomeron. This new theorem does not address the question of Regge

factorisation, which relates the properties of the pomeron in diffractive DIS to those measured in hadron-hadron reactions.

The proof of hard-scattering factorisation fails for diffractive hard processes in hadron-hadron collisions [27]. Therefore, the contribution of the resolved process to diffractive dijet photoproduction is expected to be non-factorisable. In what follows, hard-scattering factorisation is assumed to hold for both processes (direct and resolved) in the range $x_\gamma \gtrsim 0.2$. We therefore check whether a consistent set of pomeron parton densities is able to describe simultaneously the measurements of the diffractive structure function in DIS and the cross sections for diffractive dijet photoproduction within the precision of the present data.

To summarise, in this factorisable model, the pomeron is assumed to be a source of partons which interact either with the photon (in DIS and in the direct process of photoproduction) or with a partonic constituent of the photon (in the resolved process of photoproduction). Calculations based on such a model involve three basic ingredients: a) the flux of pomerons from the proton as a function of $x_{\mathcal{P}}$ and t , b) the parton densities in the pomeron, and c) the matrix elements for the hard subprocess. For the resolved process in photoproduction, a fourth ingredient is needed: the parton densities in the photon. The pomeron flux factor is extracted from hadron-hadron collisions using Regge phenomenology, and the matrix elements are computed in perturbative QCD. However, the parton densities are *a priori* unknown and have to be extracted from experiment.

In what follows, the pomeron flux factor given by Donnachie and Landshoff (DL) [3] has been used,

$$f_{\mathcal{P}/p}(x_{\mathcal{P}}, t) = \frac{9b_0^2}{4\pi^2} F_1(t)^2 x_{\mathcal{P}}^{1-2\alpha(t)} ,$$

where $F_1(t)$ is the elastic form factor of the proton, b_0 the pomeron-quark coupling ($b_0 = 1.8 \text{ GeV}^{-1}$) and $\alpha(t)$ the pomeron trajectory ($\alpha(t) = 1.085 + 0.25t$ with t in GeV^2) taken from hadron-hadron data.

The parton densities in the pomeron, $f_{i/\mathcal{P}}(\beta, \mu^2)$ with $i = q, g$, depend upon the fraction β of the pomeron momentum carried by parton i and the scale μ at which the parton structure of the pomeron is probed. In diffractive dijet photoproduction processes, one choice, which is used here, is $\mu = \hat{p}_T$, where \hat{p}_T is the transverse momentum of either of the two outgoing partons. The scale μ is set equal to Q for diffractive DIS. The parton densities in the pomeron are evolved in μ^2 according to the DGLAP equations.

In this analysis (see Section 9), the parton densities in the pomeron are determined from a simultaneous fit to the ZEUS measurements of the diffractive structure function $\tilde{F}_2^D(\beta, Q^2)$ (see below) [13] and the measurements of diffractive dijet cross sections in photoproduction presented in Section 8. The shapes of the resulting parton densities do not depend on the normalisation of the pomeron flux factor and depend only weakly on the $x_{\mathcal{P}}$ -functional form as long as this is the same in diffractive DIS and dijet photoproduction.

3.1 The diffractive structure function

For unpolarised beams, the differential cross section for diffractive DIS can be described in terms of the diffractive structure function $F_2^{D(4)}(\beta, Q^2, x_{\mathcal{P}}, t)$

$$\frac{d^4\sigma_{diff}^{DIS}}{d\beta dQ^2 dx_{\mathcal{P}} dt} = \frac{2\pi\alpha^2}{\beta Q^4} (1 + (1-y)^2) F_2^{D(4)}(\beta, Q^2, x_{\mathcal{P}}, t),$$

where α is the electromagnetic coupling constant and the contribution of the longitudinal diffractive structure function is neglected. An integration over the entire range of t defines the

diffractive structure function $F_2^{D(3)}(\beta, Q^2, x_{\mathbb{P}})$ [28] as measured in [13]:

$$\frac{d^3\sigma_{diff}^{DIS}}{d\beta dQ^2 dx_{\mathbb{P}}} = \frac{2\pi\alpha^2}{\beta Q^4} (1 + (1-y)^2) F_2^{D(3)}(\beta, Q^2, x_{\mathbb{P}}).$$

To illustrate the β and Q^2 dependence of $F_2^{D(3)}(\beta, Q^2, x_{\mathbb{P}})$, the structure function $\tilde{F}_2^D(\beta, Q^2)$ was also measured in [13]:

$$\tilde{F}_2^D(\beta, Q^2) \equiv \int_{x_{\mathbb{P}\min}}^{x_{\mathbb{P}\max}} dx_{\mathbb{P}} F_2^{D(3)}(\beta, Q^2, x_{\mathbb{P}}).$$

In the factorisable model, the diffractive structure function $F_2^{D(4)}$ is assumed to be of the form

$$F_2^{D(4)}(\beta, Q^2, x_{\mathbb{P}}, t) = f_{\mathbb{P}/p}(x_{\mathbb{P}}, t) \cdot F_2^{\mathbb{P}}(\beta, Q^2),$$

where at LO the pomeron structure function $F_2^{\mathbb{P}}$ depends on the pomeron parton densities as given by

$$F_2^{\mathbb{P}}(\beta, Q^2) = \sum_j e_j^2 \beta f_{q_j/\mathbb{P}}(\beta, Q^2).$$

In this expression, e_j is the electric charge of quark q_j and the sum runs over all quark flavours which contribute at the given value of Q^2 . Therefore, the LO calculation for \tilde{F}_2^D in this model is of the form

$$\tilde{F}_2^D(\beta, Q^2) = \sum_j e_j^2 \beta f_{q_j/\mathbb{P}}(\beta, Q^2) \cdot \int_{x_{\mathbb{P}\min}}^{x_{\mathbb{P}\max}} dx_{\mathbb{P}} dt f_{\mathbb{P}/p}(x_{\mathbb{P}}, t).$$

At next-to-leading order (NLO), $F_2^{\mathbb{P}}$ also depends on the gluon density in the pomeron. The measurements of the diffractive structure function are analysed (see Section 9) in terms of NLO QCD calculations.

3.2 Dijet cross sections in diffractive photoproduction

The dijet cross sections in diffractive photoproduction contain contributions from both the direct and resolved processes. As an example, the contribution of the direct process to the cross section for reaction (1) is given by

$$\sigma_{dir} = \int dy f_{\gamma/e}(y) \int \int dx_{\mathbb{P}} dt f_{\mathbb{P}/p}(x_{\mathbb{P}}, t) \sum_i \int d\beta \sum_{j,k} \int d\hat{p}_T^2 \frac{d\hat{\sigma}_{i+\gamma \rightarrow j+k}}{d\hat{p}_T^2}(\hat{s}, \hat{p}_T^2, \mu^2) \cdot f_{i/\mathbb{P}}(\beta, \mu^2),$$

where $f_{\gamma/e}$ is the flux of photons from the positron³. The sum in i runs over all possible types of partons present in the pomeron. The sum in j and k runs over all possible types of final state partons and $\hat{\sigma}_{i+\gamma \rightarrow j+k}$ is the cross section for the two-body collision $i + \gamma \rightarrow j + k$ and depends on the square of the centre-of-mass energy (\hat{s}), the transverse momentum of the two outgoing partons (\hat{p}_T) and the momentum scale (μ) at which the strong coupling constant ($\alpha_s(\mu^2)$) is evaluated.

³ The Q^2 dependence has been integrated out using the Weizsäcker-Williams approximation.

4 Experimental conditions

During 1994 HERA operated with protons of energy $E_p = 820$ GeV and positrons of energy $E_e = 27.5$ GeV. The ZEUS detector is described in detail in [29, 30]. The main subdetectors used in the present analysis are the central tracking system positioned in a 1.43 T solenoidal magnetic field and the uranium-scintillator sampling calorimeter (CAL). The tracking system was used to establish an interaction vertex and to cross-check the energy scale of the CAL. Energy deposits in the CAL were used to find jets and to measure jet energies. The CAL is hermetic and consists of 5918 cells each read out by two photomultiplier tubes. Under test beam conditions, the CAL has energy resolutions of $18\%/\sqrt{E}$ for electrons and $35\%/\sqrt{E}$ for hadrons. Jet energies are corrected for the energy lost in inactive material in front of the CAL. This material is typically about one radiation length. The effects of uranium noise were minimised by discarding cells in the inner (electromagnetic) or outer (hadronic) sections if they had energy deposits of less than 60 MeV or 110 MeV, respectively. The luminosity was measured from the rate of the bremsstrahlung process $e^+p \rightarrow e^+p\gamma$. A three-level trigger was used to select events online [30]. At the third level, where the full event information is available, the events were required to have at least two jets with jet transverse energy in excess of 3.5 GeV and jet pseudorapidity below 2.0 reconstructed using the CAL cell energies and positions as input to a cone algorithm (see Section 6).

5 Monte Carlo simulation

The response of the detector to jets and the correction factors for the cross sections for dijet production with a large rapidity gap were determined from Monte Carlo samples of events.

The program PYTHIA 5.7 [31] was used to generate standard (non-diffractive) hard photoproduction events for resolved and direct processes. The photon momentum spectrum was calculated using the Weizsäcker-Williams approximation. Events were generated using GRV-HO [32] for the photon parton distributions and MRSA [33] for the proton parton distributions. The partonic processes were simulated using LO matrix elements, with the inclusion of initial- and final-state parton showers. Fragmentation into hadrons was performed using the LUND string model [34] as implemented in JETSET [35]. Samples of events were generated with different values of the cutoff on the transverse momentum of the two outgoing partons, starting at $\hat{p}_{Tmin} = 2.5$ GeV.

Diffractive processes were simulated using the program POMPYT 2.5⁴ [36]. This is a Monte Carlo program where, within the framework provided by PYTHIA, the proton emits a pomeron whose partonic constituents subsequently take part in a hard scattering process with the photon or its constituents. For the resolved processes, the parton densities of the photon were parametrised according to GS-HO [37]⁵ evaluated at \hat{p}_T . The parton densities in the pomeron were parametrised according to a hard distribution $\beta(1-\beta)$ and the DL form was used for the pomeron flux factor.

All generated events were passed through the ZEUS detector and trigger simulation programs [30]. They were reconstructed and analysed by the same program chain as the data. The resulting Monte Carlo distributions agree reasonably well with the data.

⁴This version of POMPYT has been modified to make use of pomeron parton densities which evolve with the scale according to the DGLAP equations.

⁵The correction factors depend very weakly on the specific set of photon parton distributions used.

6 Jet search and reconstruction of kinematic variables

An iterative cone algorithm in the $\eta - \varphi$ plane is used to reconstruct jets from the energy measured in the CAL cells for both data and simulated events, and also from the final-state hadrons for simulated events. A detailed description of the algorithm can be found in [38]. The jets reconstructed from the CAL cell energies are called *cal* jets and the variables associated with them are denoted by $E_{T,cal}^{jet}$, η_{cal}^{jet} and φ_{cal}^{jet} . The axis of the jet is defined according to the Snowmass convention [39], where η_{cal}^{jet} (φ_{cal}^{jet}) is the transverse-energy weighted mean pseudorapidity (azimuth) of all the CAL cells belonging to that jet. The cone radius used in the jet search was set equal to 1.

For the Monte Carlo events, the same jet algorithm is also applied to the final-state particles. The jets found are called *hadron* jets and the variables associated with them are denoted by $E_{T,had}^{jet}$, η_{had}^{jet} , and φ_{had}^{jet} . *Hadron* jets with $E_{T,had}^{jet} > 6$ GeV and $-1.5 < \eta_{had}^{jet} < 1$ are selected.

The comparison of the reconstructed jet variables between the *hadron* and the *cal* jets in simulated events [40] shows no significant systematic shift in the angular variables η_{cal}^{jet} and φ_{cal}^{jet} with respect to η_{had}^{jet} and φ_{had}^{jet} . The resolutions are 0.07 units in η_{cal}^{jet} and 5° in φ_{cal}^{jet} . The transverse energy of the *cal* jet underestimates that of the *hadron* jet by an average amount of 16% with an r.m.s. of 11%. The transverse energy corrections to *cal* jets averaged over the azimuthal angle were determined using the Monte Carlo samples of events. These corrections are constructed as multiplicative factors, $C(E_{T,cal}^{jet}, \eta_{cal}^{jet})$, which, when applied to the E_T of the *cal* jets, give the true transverse energies of the jets, $E_T^{jet} = C(E_{T,cal}^{jet}, \eta_{cal}^{jet}) \times E_{T,cal}^{jet}$ [40]. These corrections mainly take into account the energy losses due to the inactive material in front of the CAL.

The γp centre-of-mass energy $W = \sqrt{y s}$ is estimated using the method of Jacquet-Blondel [41],

$$W_{JB} = \sqrt{2E_p(E - P_Z)}, \quad (2)$$

where E is the total energy as measured by the CAL, $E = \sum_i E_i$, and P_Z is the Z -component of the vector $\vec{P} = \sum_i E_i \vec{r}_i$; in both cases the sum runs over all CAL cells, E_i is the energy of the calorimeter cell i and \vec{r}_i is a unit vector along the line joining the reconstructed vertex and the geometric centre of the cell i . Due to the energy lost in the inactive material in front of the CAL and to particles lost in the rear beampipe, W_{JB} systematically underestimates the true W by approximately 13%, an effect which is adequately reproduced in the Monte Carlo simulation of the detector. Monte Carlo studies show a resolution of 6% for W_{JB} in the range $120 < W_{JB} < 251$ GeV. The reconstructed value W_{JB} is corrected to the true W by means of the Monte Carlo samples of events.

The variables of the dijet system x_{γ}^{OBS} and β^{OBS} are reconstructed as

$$x_{\gamma,cal}^{OBS} = 2E_p \frac{\sum_{jets} E_{T,cal}^{jet} e^{-\eta_{cal}^{jet}}}{W_{JB}^2}, \quad \text{and} \quad (3)$$

$$\beta_{cal}^{OBS} = \frac{\sum_{jets} E_{T,cal}^{jet} e^{\eta_{cal}^{jet}}}{2x_{\mathcal{P}}^{cal} E_p}, \quad (4)$$

where $x_{\mathcal{P}}^{cal}$ is determined from the energies and angles measured in the CAL using

$$x_{\mathcal{P}}^{cal} = \frac{E^2 - P_X^2 - P_Y^2 - P_Z^2}{W_{JB}^2}, \quad (5)$$

where P_X (P_Y) is the X (Y)-component of the vector \vec{P} . Note that in the formulae for x_γ^{OBS} and β^{OBS} many systematic uncertainties in the measurement of energy by the CAL cancel out. There are no significant systematic shifts in the variables $x_{\gamma,cal}^{OBS}$ and β_{cal}^{OBS} with respect to x_γ^{OBS} and β^{OBS} . Therefore, no corrections are needed for these variables ($x_\gamma^{OBS} \approx x_{\gamma,cal}^{OBS}$ and $\beta^{OBS} \approx \beta_{cal}^{OBS}$). The resolution in x_γ^{OBS} (β^{OBS}) is 0.06 units in the region $x_\gamma^{OBS} > 0.2$ ($\beta^{OBS} > 0.4$).

In the analysis presented here, large-rapidity-gap events are selected by using the variable η_{max}^{cal} , which is defined as the pseudorapidity of the most-forward CAL cluster exceeding 400 MeV [10]. The η_{max} variable for the Monte Carlo events at the CAL level is defined in the same way as in the data (η_{max}^{cal}). At the hadron level, η_{max}^{had} is calculated as the pseudorapidity of the most-forward particle with energy in excess of 400 MeV and pseudorapidity below 4.5 [17]. From Monte Carlo studies the resolution on η_{max}^{cal} is 0.1 units for $\eta_{max}^{cal} < 1.8$.

7 Data selection

Events from quasi-real photon-proton collisions were selected offline using criteria similar to those reported previously [17] and briefly discussed here. A search for jet structure using the CAL cells is performed and events with at least two jets of $E_T^{jet} > 6$ GeV and $-1.5 < \eta^{jet} < 1$ are retained. The contamination from beam-gas interactions, cosmic showers and beam-halo muons is negligible after imposing a cut on the vertex reconstructed from three or more tracks. Neutral current DIS events are removed from the sample by identifying the scattered positron candidate using the pattern of energy distribution in the CAL [24].

Large-rapidity-gap events are selected by using the variable η_{max}^{cal} and events with $\eta_{max}^{cal} < 1.8$ are kept for further analysis [17]. The selected sample consists of events from e^+p interactions with $Q^2 \lesssim 4$ GeV² and a median of $Q^2 \approx 10^{-3}$ GeV². The event sample is then restricted to the kinematic range $134 < W < 277$ GeV using the corrected value of W_{JB} . The data sample thus obtained consists of 403 events and represents 1.3% of the whole dijet sample in the same kinematic region except for the requirement on η_{max}^{cal} . The range in x_P spanned by the data is from 0.001 to 0.03 with a median of $x_P \approx 0.009$.

8 Dijet cross sections

Using the selected data sample of dijet events, differential dijet cross sections have been measured in the above kinematic region with the most-forward-going hadron at $\eta_{max} < 1.8$. The cross sections have been measured as a function of η^{jet} , E_T^{jet} , W , x_γ^{OBS} and β^{OBS} for dijet production with $E_T^{jet} > 6$ GeV and $-1.5 < \eta^{jet} < 1$. For each cross section, an integration over the remaining variables is implied. The cross sections refer to jets at the hadron level with a cone radius of 1 unit in the $\eta - \varphi$ plane.

The Monte Carlo samples of events generated using POMPYT were used to compute acceptance corrections to the η^{jet} , E_T^{jet} , W , x_γ^{OBS} and β^{OBS} distributions. These corrections take into account the efficiency of the trigger, the selection criteria and, the purity and efficiency of the reconstruction of jets. They also correct for the migrations in the variable η_{max}^{cal} and yield cross sections for the true rapidity gap determined by η_{max}^{had} . The cross sections are obtained by applying bin-by-bin corrections to the distributions of the data.

8.1 Background and systematic uncertainties of the measurements

The contribution from non-diffractive processes has been estimated using a sample of direct and resolved processes generated with the PYTHIA Monte Carlo⁶. The fraction of large-rapidity-gap events in PYTHIA is strongly suppressed, although fluctuations in the final-state system may give rise to a rapidity gap in the forward region in a small fraction of events. The contribution from non-diffractive processes as modelled by PYTHIA is approximately 20% in $d\sigma/dW$. This contribution, which has been subtracted bin-by-bin from the data, is listed in Table 1.

Events with diffractively dissociated protons with masses M_N less than ~ 4 GeV also contribute to the data set [13]. Since the pomeron flux factor of Donnachie and Landshoff accounts only for processes in which the proton remains intact after the collision and as the measurements are based upon a large-rapidity-gap requirement, the contribution to the measured cross sections from double dissociation has to be taken into account when comparing to model predictions. A comparison of the measurements of the diffractive structure function in DIS based on the detection of the final-state scattered proton [14] and on the M_X -method [42], shows that double dissociation with $M_N \lesssim 4$ GeV contributes $(31 \pm 13)\%$ to the cross section. This estimation has been cross-checked with a study of exclusive vector-meson production [43] yielding consistent results. Assuming Regge factorisation, the same contribution is expected to be present in the measurements of diffractive dijet photoproduction. Instead of subtracting the measurements for this contribution, the predictions of the MC program POMPYT (see next section) have been scaled up by the appropriate factor. Since this contribution affects equally the measurements of dijet cross sections and those of the diffractive structure function, the results of the QCD analysis (except for the overall normalisation) do not depend on its exact value.

The statistical errors are indicated as the inner error bars in all the figures presented below. A detailed study of the sources contributing to the systematic uncertainties of the measurements was carried out [44]. These uncertainties are classified into six groups:

- The η_{max}^{cal} variable in the data and simulated events was recomputed after removing the CAL cells with $\eta > 3.25$ in order to check the dependence on the detailed simulation of the forward region of the detector. This resulted in changes within $\pm 10\%$.
- The energy threshold in the computation of η_{max}^{cal} for data and simulated events was varied by ± 100 MeV, yielding changes within $\pm 10\%$.
- The amount of the non-diffractive contribution subtracted from the data was varied by $\pm 30\%$, yielding changes within $\pm 15\%$.
- The relative contribution of quarks and gluons in the pomeron used in the simulated events was varied within the range obtained by the QCD analysis presented in the next section. The resulting changes are below 15% except for $d\sigma/dx_\gamma^{OBS}$ in the lowest measured x_γ^{OBS} -point (+40%) and $d\sigma/d\beta^{OBS}$ in the highest measured β^{OBS} -point (-20%).
- Variations in the simulation of the trigger and a variation of the cuts used to select the data within the ranges allowed by the comparison between data and Monte Carlo simulations yielded negligible changes.

⁶These calculations give a good description of the inclusive jet differential cross sections (without the large-rapidity-gap requirement) in the range $-1 < \eta^{jet} < 1$ [40].

All these systematic uncertainties have been added in quadrature to the statistical errors and are shown as the outer error bars in the figures.

- The absolute energy scale of the *cal* jets in the simulated events was varied by $\pm 5\%$ [45], resulting in changes of approximately $\pm 25\%$. This uncertainty is the largest source of systematic error and is highly correlated between measurements at different points. It is shown as a shaded band in each figure.

In addition, there is an overall normalisation uncertainty of 1.5% from the luminosity determination which is not included. The results are presented in Table 1.

8.2 Results

The cross section $d\sigma/d\eta^{jet}$, shown in Figure 2, for the selected region of phase space has been measured in the η^{jet} range between -1.5 and 1 integrated over $E_T^{jet} > 6$ GeV. The measured cross section $d\sigma/d\eta^{jet}$ shows a broad central maximum in η^{jet} . The cross section $d\sigma/dE_T^{jet}$ measured in the range of E_T^{jet} between 6 and 14 GeV and integrated over $-1.5 < \eta^{jet} < 1$ is presented in Figure 3. The cross section $d\sigma/dE_T^{jet}$ shows a steep fall-off as a function of E_T^{jet} . Note that in the data of Figures 2 and 3 each of the two jets with highest E_T^{jet} in an event contributes to the cross section.

The cross section $d\sigma/dW$ for the selected region of phase space has been measured in the W range between 134 GeV and 277 GeV. The cross section, shown in Figure 4, falls for low values of W but remains fairly constant for large values of W .

The cross section $d\sigma/dx_\gamma^{OBS}$ has been measured in the x_γ^{OBS} range between 0.2 and 1 . The cross section $d\sigma/dx_\gamma^{OBS}$, shown in Figure 5, peaks at high values of x_γ^{OBS} with a pronounced tail that extends to low- x_γ^{OBS} values. This result shows the presence of both a resolved- (low- x_γ^{OBS}) and a direct-photon (high- x_γ^{OBS}) component in diffractive dijet photoproduction.

The cross section $d\sigma/d\beta^{OBS}$, measured in the β^{OBS} range between 0.4 and 1 , is shown in Figure 6. The cross section increases as β^{OBS} increases and shows that there is a sizeable contribution to dijet production from those events in which a large fraction of the pomeron momentum participates in the hard scattering.

The results are compared with the predictions of the MC program POMPYT using various parton distributions which are described in the following section.

9 QCD analysis

A combined QCD analysis of the ZEUS measurements of the diffractive structure function $\tilde{F}_2^D(\beta, Q^2)$ in DIS [13] and of the measured dijet cross sections in diffractive photoproduction presented in the previous section has been performed following the proposal by Collins et al. [46]. This procedure assumes both hard-scattering factorisation and Regge factorisation of pomeron exchange in diffractive DIS and diffractive dijet photoproduction.

The diffractive structure function $\tilde{F}_2^D(\beta, Q^2)$ was measured [13] for Q^2 values between 10 and 63 GeV², and β values between 0.175 and 0.65 , by means of an integration over the measured range of x_P , $6.3 \cdot 10^{-4} < x_P < 10^{-2}$. The fits to the DIS data are based on full NLO QCD calculations. On the other hand, the fits to the photoproduction data use calculations with LO matrix elements plus parton-shower as incorporated in POMPYT. Both direct and resolved processes are included.

In the calculations of the diffractive dijet cross sections using POMPYT, $\alpha_s(\mu^2)$ and the parton densities in the pomeron and the photon are evaluated at $\mu^2 = \hat{p}_T^2$. These computations may be affected by higher-order QCD corrections, which are expected to mainly change the normalisation (i.e. generate a K -factor). The agreement found between the PYTHIA calculations of the inclusive jet differential cross sections and the ZEUS measurements [40] indicates that in the case of the non-diffractive contribution the K -factor is close to unity, within an uncertainty of $\pm 30\%$. The K -factor in the case of POMPYT is expected to be similar (with a similar uncertainty), as the same hard subprocesses are involved in the calculation of the jet cross sections.

Each of the fits is represented by a parametrisation of the initial distributions at $\mu_0^2 = 4 \text{ GeV}^2$ for the quarks ($f_{u/\mathbb{P}}(\beta, \mu^2) = f_{\bar{u}/\mathbb{P}} = f_{d/\mathbb{P}} = f_{\bar{d}/\mathbb{P}}$) and for the gluon ($f_{g/\mathbb{P}}$). The other quark distributions are assumed to be zero at the initial scale. The parton distributions are evolved in μ^2 according to the DGLAP equations at NLO with the number of flavours set equal to five, the \overline{MS} -scheme with $\Lambda_{\overline{MS}}^{(5)} = 152 \text{ MeV}$ and using the program from the CTEQ group [47].

The fits were performed simultaneously to the 1993 ZEUS measurements of $\tilde{F}_2^D(\beta, Q^2)$ (Figure 7) and the measured cross sections $d\sigma/d\eta^{jet}$ (Figure 2) and $d\sigma/d\beta^{OBS}$ (Figure 6) in diffractive photoproduction. These cross sections in diffractive photoproduction are those which are most sensitive to the shape of the pomeron parton densities. The following functional forms for the momentum-weighted parton densities in the pomeron at μ_0^2 have been used in the fits:

- hard quark + hard gluon:

$$\beta f_{u/\mathbb{P}}(\beta, \mu_0^2) = a_1 \beta (1 - \beta) \quad , \quad \beta f_{g/\mathbb{P}}(\beta, \mu_0^2) = b_1 \beta (1 - \beta);$$

- hard quark + leading gluon:

$$\beta f_{u/\mathbb{P}}(\beta, \mu_0^2) = a_2 \beta (1 - \beta) \quad , \quad \beta f_{g/\mathbb{P}}(\beta, \mu_0^2) = b_2 \beta^8 (1 - \beta)^{0.3},$$

- hard quark + (hard & leading) gluon:

$$\beta f_{u/\mathbb{P}}(\beta, \mu_0^2) = a_3 \beta (1 - \beta) \quad , \quad \beta f_{g/\mathbb{P}}(\beta, \mu_0^2) = b_3 \beta (1 - \beta) + c_3 \beta^8 (1 - \beta)^{0.3},$$

where the values of a_i , b_i and c_i are determined from the fits. Note that all these functional forms are constrained to be zero at $\beta = 1$. The exact shape of the parton distributions are only weakly constrained for $\beta \gtrsim 0.8$.

The fraction of the pomeron momentum carried by partons is defined as

$$\Sigma_{\mathbb{P}}^{NLO} \equiv \int_0^1 d\beta \beta [f_{g/\mathbb{P}}(\beta, \mu^2) + \sum_j f_{q_j/\mathbb{P}}(\beta, \mu^2)],$$

where the sum runs over all quark flavours which contribute at the given value of μ^2 . Since the pomeron is not a particle it is unclear whether or not the momentum sum rule ($\Sigma_{\mathbb{P}}^{NLO} = 1$) should be satisfied. Therefore, $\Sigma_{\mathbb{P}}^{NLO}$ has been left unconstrained in the fits.

The functional form of the ‘‘leading gluon’’ distribution is similar to one of the parametrisations extracted by the H1 Collaboration from the observed scaling violations of the diffractive structure function [15]. Parametrisations of the parton densities in which the pomeron is assumed to be made exclusively of quarks have been disfavoured by previous measurements [15,17] and are not considered here. Likewise, a parametrisation of the gluon density with a soft spectrum has been ruled out [15,17,48].

The fitted values of the parameters are shown in Table 2. These values have been obtained by subtracting from the data an estimated $(31 \pm 13)\%$ contribution due to double dissociation. In the figures, the results of the fits have been scaled up to take into account this contribution. The results of the three different fits are compared to the measurements used for the fits in Figures 2, 6 and 7. The calculations based on these fits, which include a substantial hard momentum component of gluons at μ_0^2 in the pomeron, give a reasonable description of the shape and normalisation of the measurements. The measured $d\sigma/d\beta^{OBS}$ rises as β^{OBS} increases while the calculations fall at $\beta^{OBS} \gtrsim 0.8$ for the parton distributions chosen. This comparison indicates that there is a sizeable contribution of gluons at large β .

The results of the fits have also been compared to those dijet cross sections in diffractive photoproduction which were not used in the fit (Figures 3 to 5). The calculations provide a good description of the measured $d\sigma/dE_T^{jet}$, $d\sigma/dW$ and $d\sigma/dx_\gamma^{OBS}$. The sensitivity of the measured $d\sigma/dW$ to the value of $\alpha(0)$ in the pomeron trajectory is limited due to the cut on E_T^{jet} used to define the jets and the requirement on η_{max} . These comparisons are consistent with the conclusion that there is a large component of gluons with a hard momentum spectrum in the pomeron. Moreover, the measured $d\sigma/dE_T^{jet}$ is well described by the calculations, indicating that the dynamics of dijet diffractive photoproduction is governed by the matrix elements of perturbative QCD.

The predicted contributions from direct and resolved processes to the measured $d\sigma/dx_\gamma^{OBS}$, together with their sum, are shown in Figure 5. The sum of the contributions from resolved and direct processes gives a good description of the data. The shape of the contribution of either a purely direct-photon or a purely resolved-photon is not able to reproduce the data. A resolved-photon component is therefore needed in order to explain the shape of the measured cross section for values of x_γ^{OBS} below 0.8. This observation represents the first clear experimental evidence for the presence of both a resolved- and a direct-photon component in diffractive dijet photoproduction. Hard-scattering factorisation-breaking effects due to the resolved-photon component might be suppressed by the observed dominance of the direct-photon contribution to diffractive dijet photoproduction in the selected region of phase space.

The fraction of the pomeron momentum carried by partons which is due to gluons,

$$c_g^{NLO}(\mu^2) \equiv \frac{1}{\Sigma_{\mathbb{P}}^{NLO}} \int_0^1 d\beta \beta f_{g/\mathbb{P}}(\beta, \mu^2),$$

depends upon the scale at which the parton content of the pomeron is probed and has been computed for each of the fits. The determination of $c_g^{NLO}(\mu^2)$ is affected by the following uncertainties:

- The statistical and systematic uncertainties of the measurements used in the fits, which are the dominant sources of uncertainty.
- The uncertainty ($\pm 30\%$) on the POMPYT calculations due to higher-order QCD corrections.
- The uncertainty on the pomeron trajectory in the DL pomeron flux factor. The effect on $c_g^{NLO}(\mu^2)$ has been estimated by changing $\alpha(0)$ from 1.085 to 1.15.

The central value of $c_g^{NLO}(4 \text{ GeV}^2)$ varies between 0.75 and 0.90 depending on the parametrisation and is given in Table 2. Taking into account all the uncertainties of the three fits, the resulting range for c_g^{NLO} is $0.64 < c_g^{NLO}(4 \text{ GeV}^2) < 0.94$.

The fraction $c_g^{NLO}(\mu^2)$ has also been computed at the μ^2 values probed⁷ by other measurements and is shown in Figure 8: a) $\mu^2 = (E_T^{jet})^2 = (6 \text{ GeV})^2 = 36 \text{ GeV}^2$ in dijet diffractive photoproduction (this analysis); b) $\mu^2 = (E_T^{jet})^2 = (8 \text{ GeV})^2 = 64 \text{ GeV}^2$ in inclusive jet diffractive photoproduction [17]; c) $\mu^2 = (E_T^{jet})^2 = (20 \text{ GeV})^2 = 400 \text{ GeV}^2$ in dijet diffractive production in $\bar{p}p$ [19]; and d) $\mu^2 = M_W^2 = 6400 \text{ GeV}^2$ in diffractive W -boson production in $\bar{p}p$ [18].

The result for c_g^{NLO} is consistent with the previous determination by ZEUS [17] though now with an improved method and accuracy. The extrapolation of this result to the μ^2 values probed by the measurements in $\bar{p}p$ collisions is also consistent with the estimate of $(70 \pm 20)\%$ given by the CDF Collaboration [19]. However, care must be taken in these comparisons since the result presented here has been made using pomeron parton densities which depend upon the scale according to the DGLAP equations while those in [17] and [19] neglected any scale dependence. The use of different procedures does not have a significant effect on the extracted values of c_g , but affects substantially the values of $\Sigma_{\bar{p}}$.

We conclude that for the selected region of phase space, which includes the η_{max} requirement, and within our experimental uncertainties it is possible to reproduce the measurements of the diffractive structure function [13] and of the dijet cross sections in diffractive photoproduction with the Ingelman-Schlein model [1]. In this model, which assumes Regge factorisation, the parton densities of the pomeron evolve according to the DGLAP equations. The dominance of the direct process for the measured region of phase space could be limiting the observation of hard-scattering factorisation-breaking effects due to the resolved-photon component. The data require the fraction of the pomeron momentum carried by partons which is due to gluons to lie in the range $0.64 < c_g^{NLO}(4 \text{ GeV}^2) < 0.94$.

10 Summary and conclusions

Measurements of the differential cross sections for dijet photoproduction with a large rapidity gap in e^+p collisions at a centre-of-mass energy of 300 GeV have been presented. The e^+p dijet cross sections refer to jets at the hadron level with a cone radius of one unit in the $\eta - \varphi$ plane. They are given in the kinematic region defined by $Q^2 \leq 4 \text{ GeV}^2$ (with a median $Q^2 \approx 10^{-3} \text{ GeV}^2$) and $134 < W < 277 \text{ GeV}$ with the most-forward-going hadron at $\eta_{max} < 1.8$. These cross sections have been measured as a function of η^{jet} , E_T^{jet} and W for dijet production with $E_T^{jet} > 6 \text{ GeV}$ and $-1.5 < \eta^{jet} < 1$.

The measured cross section $d\sigma/dx_\gamma^{OBS}$ as a function of x_γ^{OBS} , the fraction of the photon momentum participating in the production of the two jets with highest E_T^{jet} , peaks at $x_\gamma^{OBS} \sim 1$ with a pronounced tail to lower values. This result is clear evidence for resolved- and direct-photon components in diffractive dijet photoproduction.

A measurement of the cross section for diffractive dijet photoproduction as a function of β^{OBS} , the fraction of the pomeron momentum participating in the production of the two jets with highest E_T^{jet} , has been presented. For the selected region of phase space the measured cross section $d\sigma/d\beta^{OBS}$ increases as β^{OBS} increases. This result shows that there is a sizeable contribution to dijet production from those events in which a large fraction of the pomeron momentum participates in the hard scattering.

A QCD analysis of the measurements of the diffractive structure function in DIS [13] and

⁷For the non-DIS measurements referred to here the μ^2 value is not uniquely defined and c_g^{NLO} has been computed at either $(E_T^{jet})^2$ or the square of the W -boson mass depending on the specific final state.

of the measured cross sections $d\sigma/d\eta^{jet}$ and $d\sigma/d\beta^{OBS}$ presented here has been performed. The pomeron is assumed to have hadron-like partonic structure in the form of parton densities which evolve according to the DGLAP equations. It is possible to reproduce both sets of measurements when a substantial hard momentum component of gluons in the pomeron at the initial scale of 2 GeV is included. The data require the fraction of the pomeron momentum carried by partons which is due to gluons to lie in the range $0.64 < c_g^{NLO}(4 \text{ GeV}^2) < 0.94$.

Acknowledgements

The strong support and encouragement of the DESY Directorate have been invaluable. The experiment was made possible by the inventiveness and the diligent efforts of the HERA machine group. The design, construction and installation of the ZEUS detector have been made possible by the ingenuity and dedicated efforts of many people from inside DESY and from the home institutes who are not listed as authors. Their contributions are acknowledged with great appreciation. We would like to thank L. Alvero and J.C. Collins for valuable discussions.

References

- [1] G. Ingelman and P.E. Schlein, Phys. Lett. B152 (1985) 256.
- [2] E.L. Berger et al., Nucl. Phys. B286 (1987) 704.
- [3] A. Donnachie and P.V. Landshoff, Nucl. Phys. B303 (1988) 634.
- [4] K.H. Streng, Proc. of HERA Workshop, DESY (1987) 365.
- [5] N.N. Nikolaev and B.G. Zakharov, Z. Phys. C53 (1992) 331.
- [6] A. Donnachie and P.V. Landshoff, Phys. Lett. B285 (1992) 172.
- [7] J.C. Collins, L. Frankfurt and M. Strikman, Phys. Lett. B307 (1993) 161.
- [8] A. Berera and D.E. Soper, Phys. Rev. D50 (1994) 4328.
- [9] UA8 Collab., A. Brandt et al., Phys. Lett. B211 (1988) 239, B297 (1992) 417.
- [10] ZEUS Collab., M. Derrick et al., Phys. Lett. B315 (1993) 481, Phys. Lett. B332 (1994) 228.
- [11] H1 Collab., T. Ahmed et al., Nucl. Phys. B429 (1994) 477.
- [12] H1 Collab., T. Ahmed et al., Phys. Lett. B348 (1995) 681.
- [13] ZEUS Collab., M. Derrick et al., Z. Phys. C68 (1995) 569.
- [14] ZEUS Collab., J. Breitweg et al., Eur. Phys. J. C1 (1998) 81.
- [15] H1 Collab., C. Adloff et al., Z. Phys. C76 (1997) 613.
- [16] L.N. Lipatov, Sov. J. Nucl. 20 (1975) 95; V.N. Gribov and L.N. Lipatov, Sov. J. Nucl. Phys. 15 (1972) 438; G. Altarelli and G. Parisi, Nucl. Phys. B126 (1977) 298; Yu. L. Dokshitzer, Sov. Phys. JETP 46 (1977) 641.

- [17] ZEUS Collab., M. Derrick et al., Phys. Lett. B356 (1995) 129.
- [18] CDF Collab., F. Abe et al., Phys. Rev. Lett. 78 (1997) 2698.
- [19] CDF Collab., F. Abe et al., Phys. Rev. Lett. 79 (1997) 2636.
- [20] L. Alvero, J.C. Collins, J. Terron and J. Whitmore, “Diffractive Production of Jets and Weak Bosons, and Tests of Hard Scattering Factorization”, preprint CTEQ-701 (hep-ph/9701374).
- [21] K. Goulianos, “Factorization and Scaling in Hard Diffraction”, talk given at 5th International Workshop on Deep Inelastic Scattering and QCD (DIS 97), Chicago, IL, 14-18 April 1997 (hep-ph/9701374).
- [22] J.F. Owens, Phys. Rev. D21 (1980) 54.
- [23] W.J. Stirling and Z. Kunszt, Proceedings of the HERA Workshop (1987) 331; M. Drees and F. Halzen, Phys. Rev. Lett. 61 (1988) 275; M. Drees and R.M. Godbole, Phys. Rev. D39 (1989) 169.
- [24] ZEUS Collab., M. Derrick et al., Phys. Lett. B322 (1994) 287.
- [25] ZEUS Collab., M. Derrick et al., Phys. Lett. B348 (1995) 665.
- [26] J.C. Collins, D.E. Soper and G. Sterman, Nucl. Phys. B261 (1985) 104 and B308 (1988) 833; G.T. Bodwin, Phys. Rev. D31 (1985) 2616 and D34 (1986) 3932.
- [27] J.C. Collins, “Proof of Factorization for Diffractive Hard Scattering”, Preprint PSU/TH/189 (hep-ph/9709499) and references therein.
- [28] G. Ingelman and K. Jansen-Prytz, Z. Phys. C58 (1993) 285.
- [29] ZEUS Collab., M. Derrick et al., Phys. Lett. B293 (1992) 465.
- [30] The ZEUS Detector, Status Report (1993), DESY 1993.
- [31] H.-U. Bengtsson and T. Sjöstrand, Comp. Phys. Comm. 46 (1987) 43; T. Sjöstrand, Comp. Phys. Comm. 82 (1994) 74.
- [32] M. Glück, E. Reya and A. Vogt, Phys. Rev. D46 (1992) 1973.
- [33] A.D. Martin, W.J. Stirling and R.G. Roberts, Phys. Rev. D50 (1994) 6734.
- [34] B. Andersson et al., Phys. Rep. 97 (1983) 31.
- [35] T. Sjöstrand, Comp. Phys. Comm. 39 (1986) 347; T. Sjöstrand and M. Bengtsson, Comp. Phys. Comm. 43 (1987) 367.
- [36] P. Bruni and G. Ingelman, Proc. of the International Europhysics Conference, edited by J. Carr and M. Perrotet, Marseille, France, July 1993 (Ed. Frontiers, Gif-sur-Yvette, 1994), p. 595.
- [37] L.E. Gordon and J.K. Storrow, Z. Phys. C56 (1992) 307.

- [38] ZEUS Collab., J. Breitweg et al., Eur. Phys. J. C2 (1998) 61.
- [39] J. Huth et al., Proc. of the 1990 DPF Summer Study on High Energy Physics, Snowmass, Colorado, edited by E.L. Berger (World Scientific, Singapore,1992) p. 134.
- [40] ZEUS Collab., M. Derrick et al., Phys. Lett. B342 (1995) 417.
- [41] Method proposed by F. Jacquet and A. Blondel in Proc. of the Study for an *ep* Facility for Europe, U. Amaldi et al., DESY 79/48 (1979) 377.
- [42] ZEUS Collab., “Measurement of the Diffractive Cross Section in DIS at HERA”, contributed paper N-638 to the International Europhysics Conference on High Energy Physics, Jerusalem, Israel, 1997.
- [43] ZEUS Collab., “Exclusive Vector Meson production in DIS at HERA”, contributed paper N-639 to the International Europhysics Conference on High Energy Physics, Jerusalem, Israel, 1997.
- [44] J. Puga, Ph.D. Thesis, Universidad Autónoma de Madrid (1998).
- [45] ZEUS Collab., J. Breitweg et al., Eur. Phys. J. C1 (1998) 109.
- [46] J.C. Collins et al., Phys. Rev. D51 (1995) 3182; see also [20].
- [47] CTEQ Collab., R. Brock et al., Rev. Mod. Phys. 67 (1995) 157.
- [48] H1 Collab., T. Ahmed et al., Nucl. Phys. B435 (1995) 3.

η^{jet} -range	Bin centre	$d\sigma/d\eta^{jet}$ [pb]	\pm stat.	\pm syst.	syst. E_T^{jet} -scale [pb]	non-diff. subtr. [pb]
(-1.5,-1)	-1.25	75	± 8	± 13	(+25,-17)	10
(-1,-0.5)	-0.75	118	± 10	± 22	(+30,-22)	24
(-0.5,0)	-0.25	141	± 11	± 21	(+29,-23)	31
(0,0.5)	0.25	114	± 9	± 20	(+25,-18)	35
(0.5,1)	0.75	70	± 7	± 13	(+17,-13)	24
E_T^{jet} -range [GeV]	weighted mean [GeV]	$d\sigma/dE_T^{jet}$ [pb/GeV]	\pm stat.	\pm syst.	syst. E_T^{jet} -scale [pb/GeV]	non-diff. subtr. [pb/GeV]
(6,8)	6.9	97	± 5	± 16	(+22,-18)	17
(8,10)	8.8	25.2	± 1.7	± 3.7	(+6.2,-4.0)	9.0
(10,12)	10.7	7.4	± 1.0	± 1.9	(+2.1,-1.5)	3.1
(12,14)	12.8	2.1	± 0.5	± 0.7	(+0.5,-0.5)	1.3
W -range [GeV]	Bin centre [GeV]	$d\sigma/dW$ [pb/GeV]	\pm stat.	\pm syst.	syst. E_T^{jet} -scale [pb/GeV]	non-diff. subtr. [pb/GeV]
(134,170)	152	0.43	± 0.07	± 0.13	(+0.16,-0.10)	0.11
(170,206)	188	0.98	± 0.12	± 0.15	(+0.24,-0.18)	0.19
(206,241)	223	1.02	± 0.12	± 0.20	(+0.23,-0.17)	0.27
(241,277)	259	1.14	± 0.09	± 0.22	(+0.25,-0.19)	0.29
x_γ^{OBS} -range	Bin centre	$d\sigma/dx_\gamma^{OBS}$ [pb]	\pm stat.	\pm syst.	syst. E_T^{jet} -scale [pb]	non-diff. subtr. [pb]
(0.2,0.4)	0.3	13.6	± 3.6	± 7.5	(+9.8,-4.6)	8.8
(0.4,0.6)	0.5	57	± 9	± 15	(+11,-11)	35
(0.6,0.8)	0.7	162	± 17	± 27	(+41,-25)	46
(0.8,1.0)	0.9	373	± 30	± 67	(+62,-52)	64
β^{OBS} -range	Bin centre	$d\sigma/d\beta^{OBS}$ [pb]	\pm stat.	\pm syst.	syst. E_T^{jet} -scale [pb]	non-diff. subtr. [pb]
(0.4,0.55)	0.48	115	± 20	± 26	(+27,-20)	6
(0.55,0.7)	0.63	128	± 20	± 28	(+36,-26)	22
(0.7,0.85)	0.78	279	± 29	± 56	(+59,-51)	54
(0.85,1.0)	0.93	330	± 35	± 78	(+58,-40)	73

Table 1: Measured cross sections in the kinematic region defined by $Q^2 \leq 4 \text{ GeV}^2$ and $134 < W < 277 \text{ GeV}$ with the most-forward-going hadron at $\eta_{max} < 1.8$. The contribution from non-diffractive processes, which is given in the last column, has been subtracted. The measurements contain an estimated $(31 \pm 13)\%$ contribution from double dissociation. The statistical and systematic uncertainties –not associated with the absolute energy scale of the jets– are also indicated. The systematic uncertainties associated to the absolute energy scale of the jets are quoted separately. The overall normalisation uncertainty of 1.5% from the luminosity determination is not included.

i	Parametrisation	a_i	b_i	c_i	$c_g^{NLO}(4 \text{ GeV}^2)$	Σ_P^{NLO}	χ_{stat}^2/dof
1	hard quark + hard gluon	0.30	10.5	-	0.90	1.96	49/18
2	hard quark + leading gluon	0.34	13.2	-	0.75	0.89	53/18
3	hard quark + (hard & leading) gluon	0.32	5.74	6.31	0.86	1.49	33/17

Table 2: Fitted values of the parameters for each of the three fits discussed in the text. The values of $c_g^{NLO}(4 \text{ GeV}^2)$, Σ_P^{NLO} and χ_{stat}^2 , and the number of degrees of freedom (dof) for each of the fits are also shown.

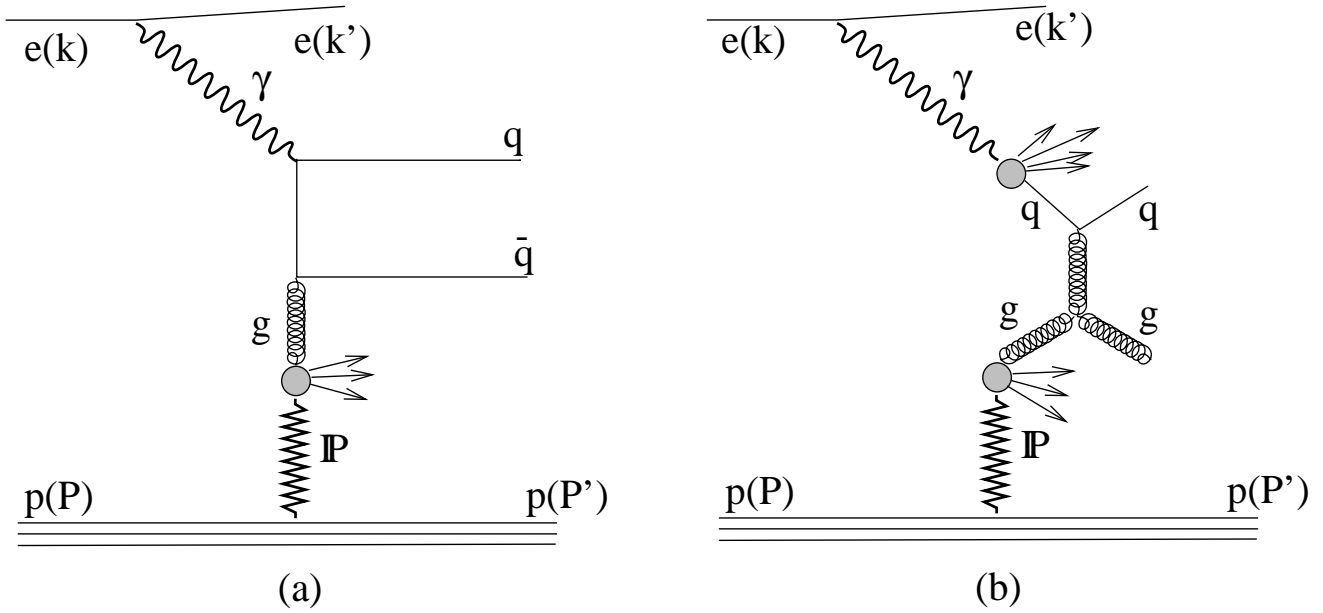


Figure 1: Examples of Feynman diagrams for diffractive dijet photoproduction: a) direct process and b) resolved process.

ZEUS 1994

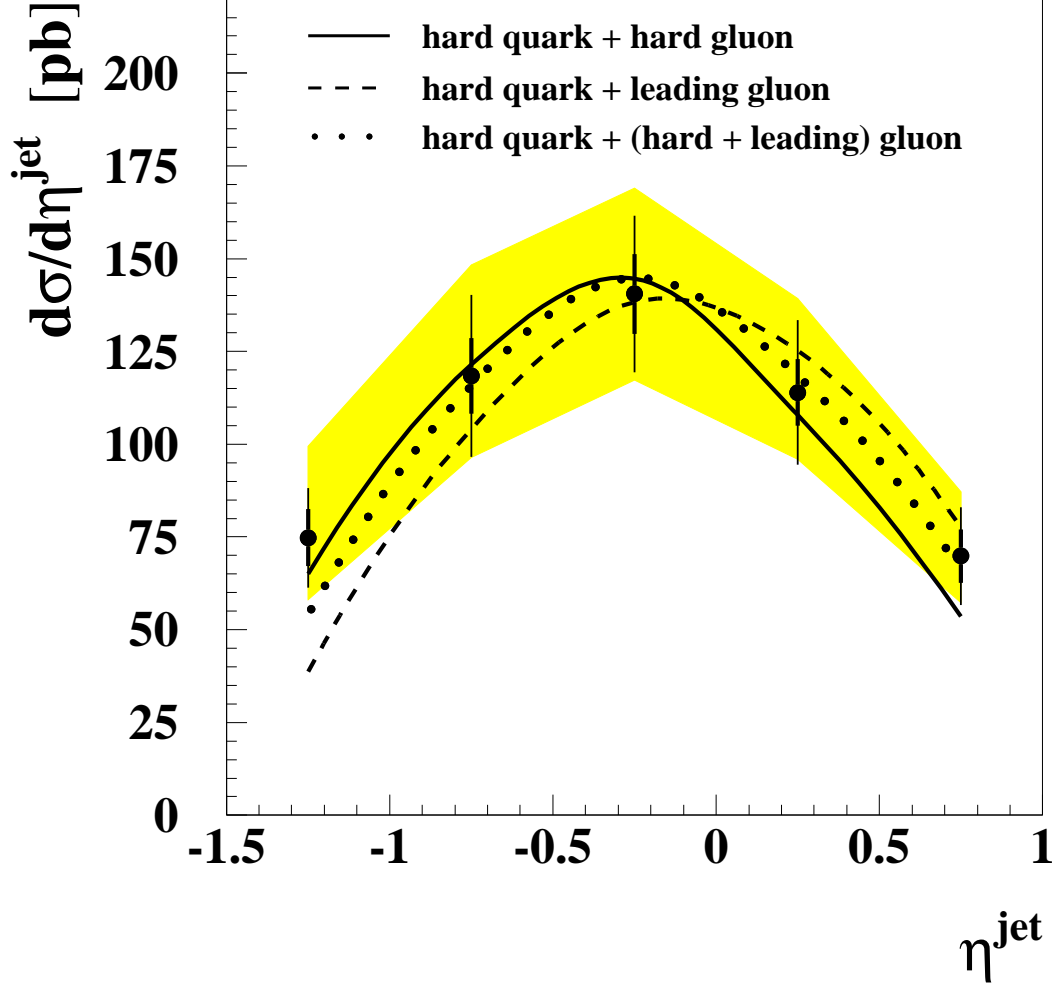


Figure 2: Measured jet cross section $d\sigma/d\eta^{\text{jet}}$ in dijet events (see text) integrated over $E_T^{\text{jet}} > 6$ GeV in the kinematic region defined by $Q^2 \leq 4$ GeV² and $134 < W < 277$ GeV with the most-forward-going hadron at $\eta_{\text{max}} < 1.8$ (black dots). The contribution from non-diffractive processes (see Table 1) has been subtracted. The measurements contain an estimated $(31 \pm 13)\%$ contribution from double dissociation. The inner error bars represent the statistical errors of the data, and the outer error bars show the statistical and systematic uncertainties –not associated with the absolute energy scale of the jets– added in quadrature. The shaded band displays the uncertainty due to the absolute energy scale of the jets. For comparison, the results of the QCD fits, which have been scaled up to account for the contribution from double dissociation, are shown (see text). The results of the QCD fits have been obtained by an integration over the same bins as for the data and are presented as smooth curves joining the calculated points.

ZEUS 1994

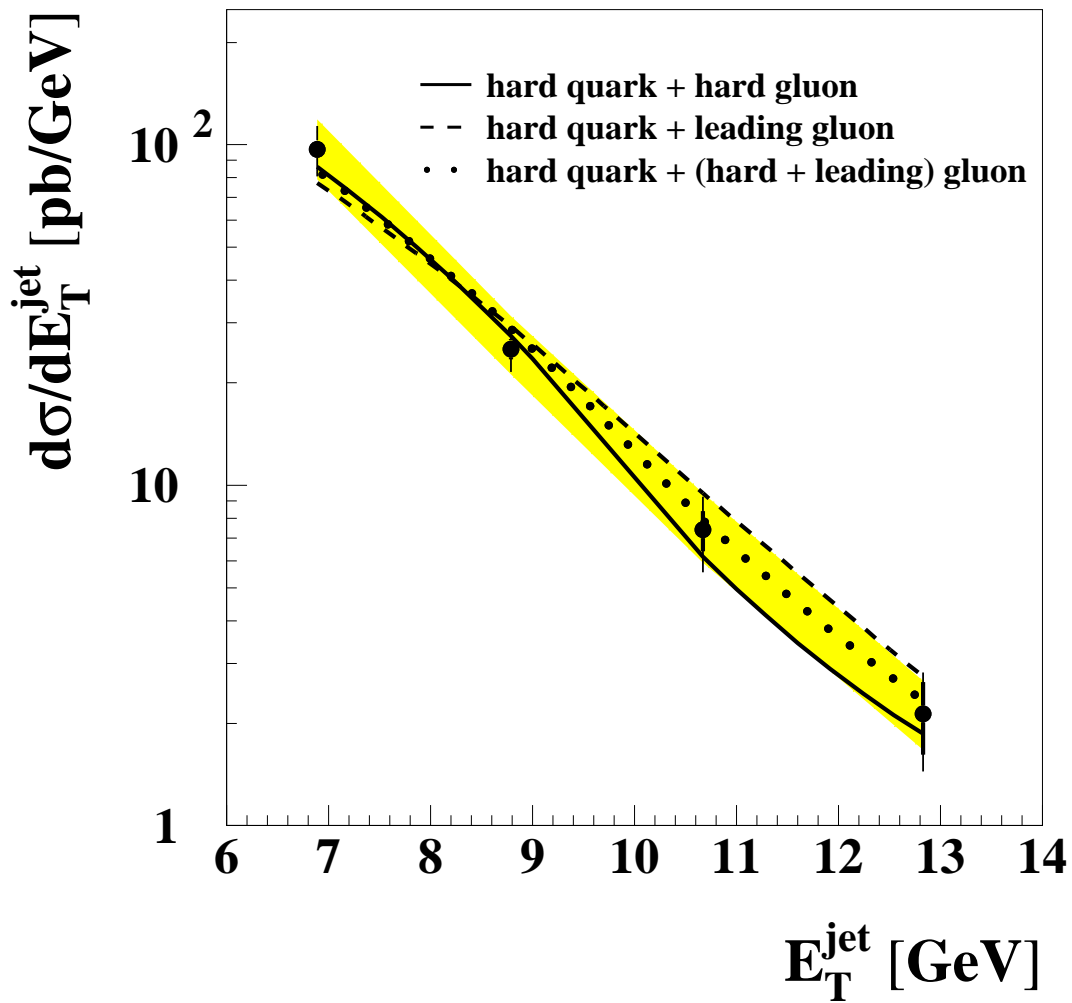


Figure 3: Measured jet cross section $d\sigma/dE_T^{\text{jet}}$ in dijet events (see text) integrated over $-1.5 < \eta^{\text{jet}} < 1$. Other details as in Figure 2.

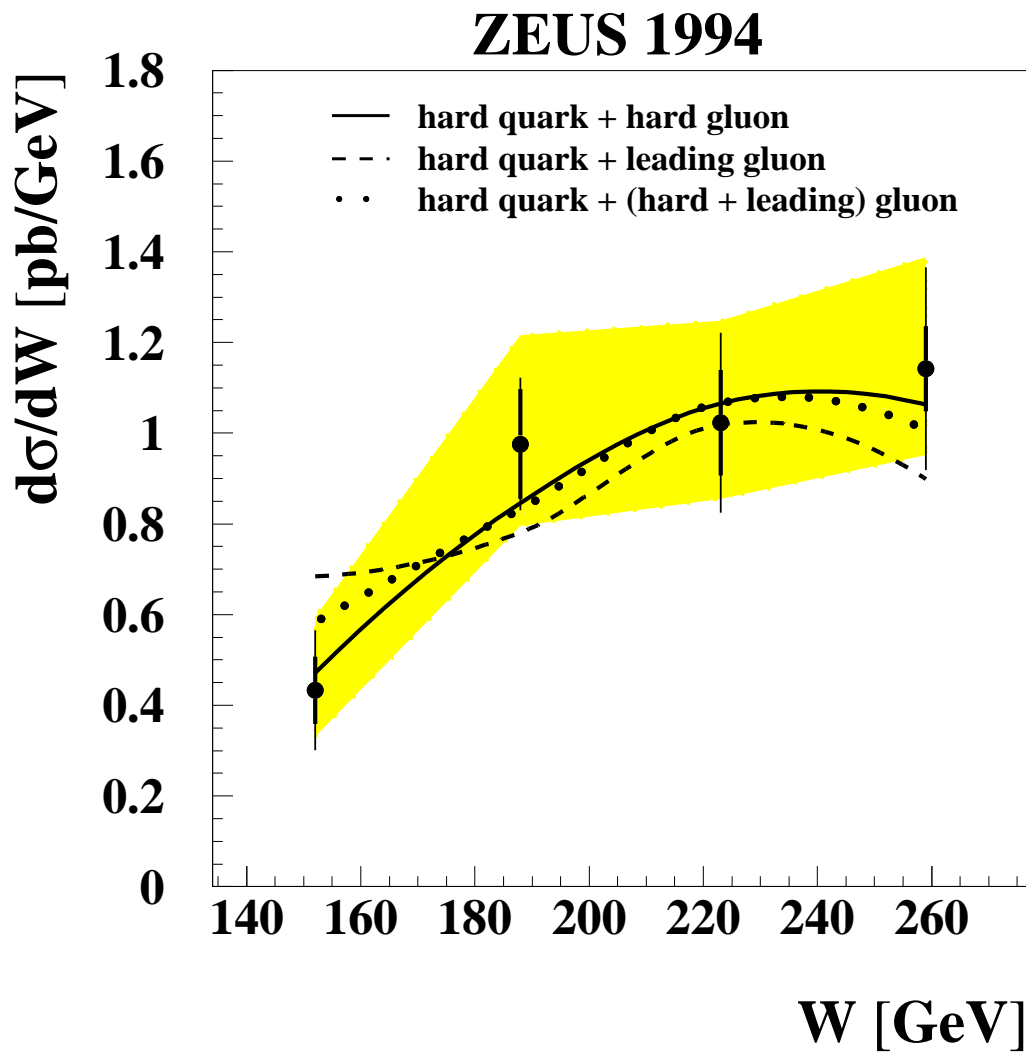


Figure 4: Measured dijet cross section $d\sigma/dW$ integrated over $E_T^{jet} > 6$ GeV and $-1.5 < \eta^{jet} < 1$. Other details as in Figure 2.

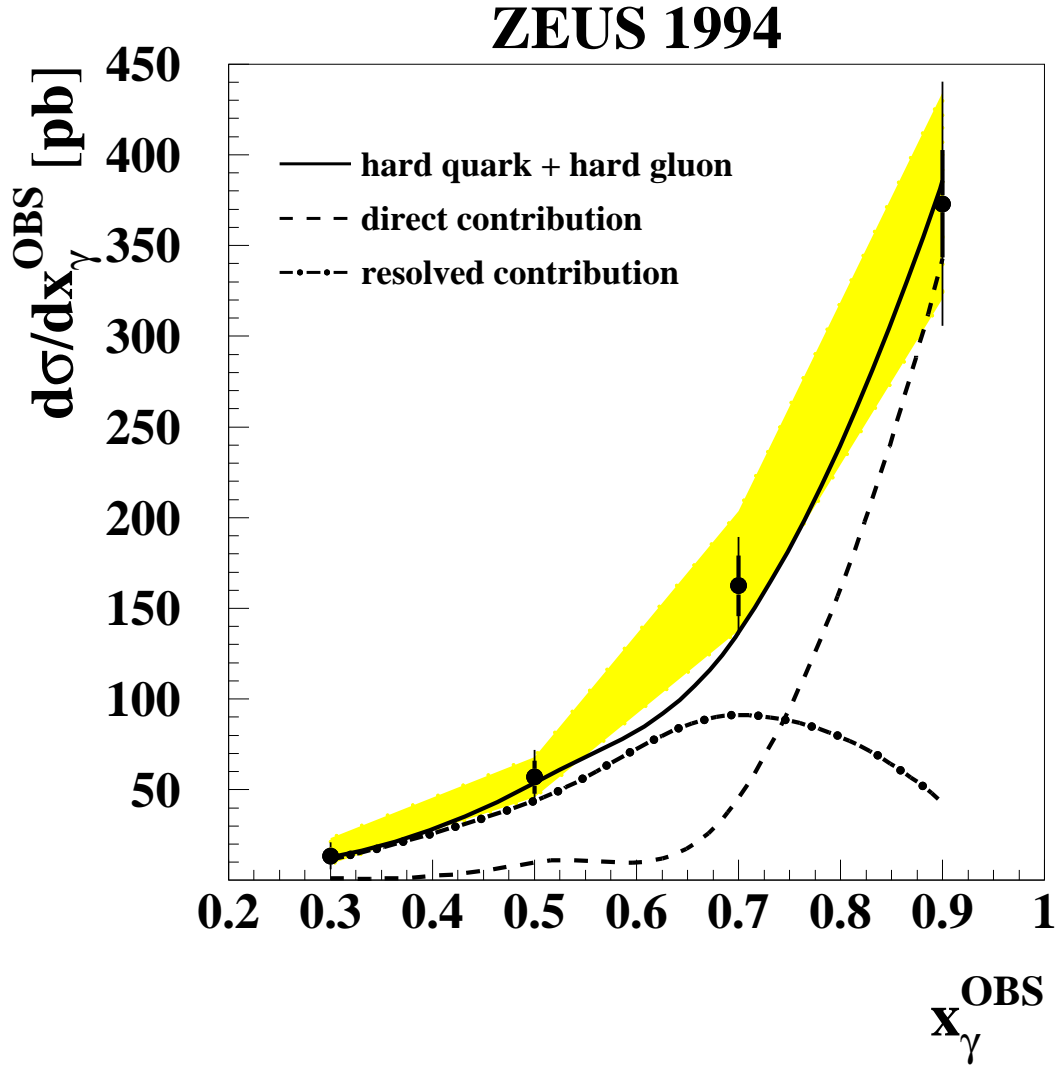


Figure 5: Measured dijet cross section $d\sigma/dx_\gamma^{OBS}$ integrated over $E_T^{jet} > 6$ GeV and $-1.5 < \eta^{jet} < 1$. Other details as in Figure 2. For comparison, the calculations for the resolved (dot-dashed line), direct (dashed line) and resolved plus direct processes (solid line) based on the QCD fit with the “hard quark + hard gluon” parametrisation (see text) are shown.

ZEUS 1994

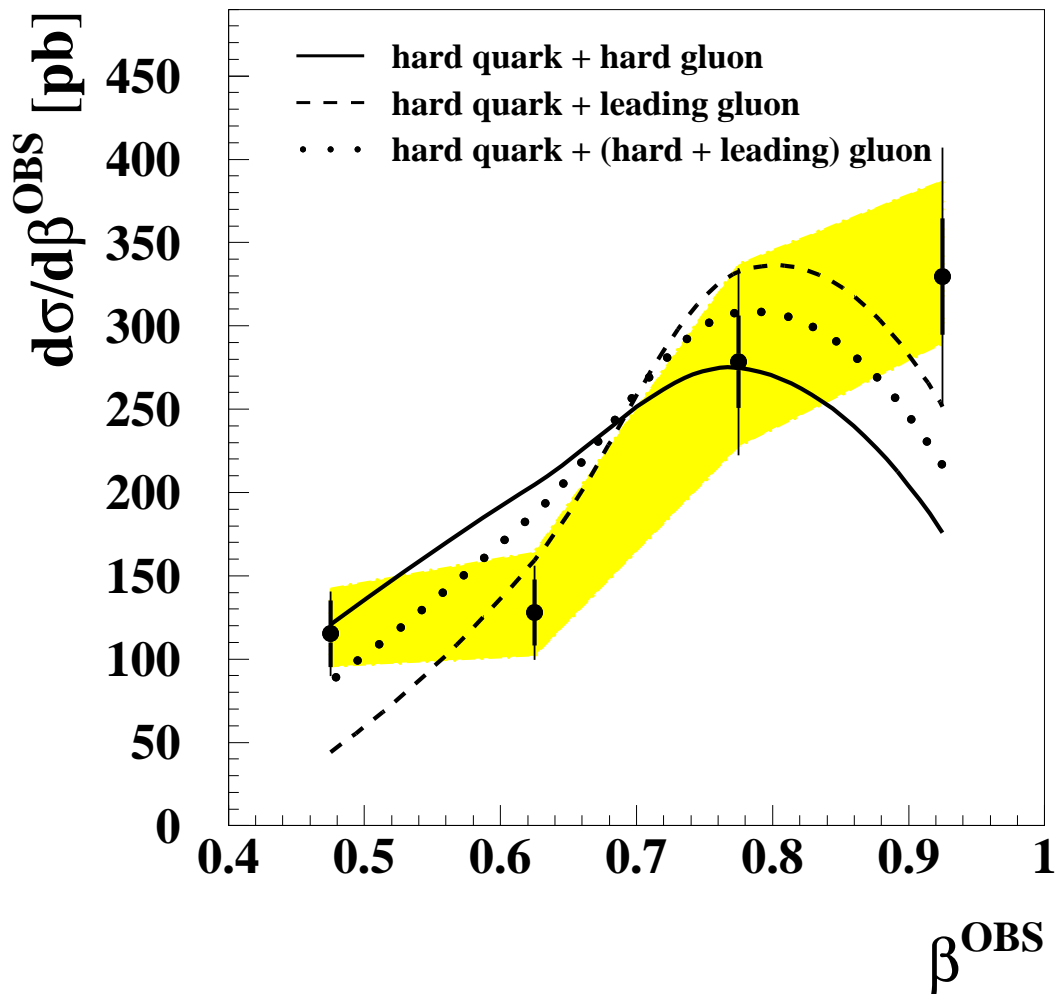


Figure 6: Measured dijet cross section $d\sigma/d\beta^{OBS}$ integrated over $E_T^{jet} > 6$ GeV and $-1.5 < \eta^{jet} < 1$. Other details as in Figure 2.

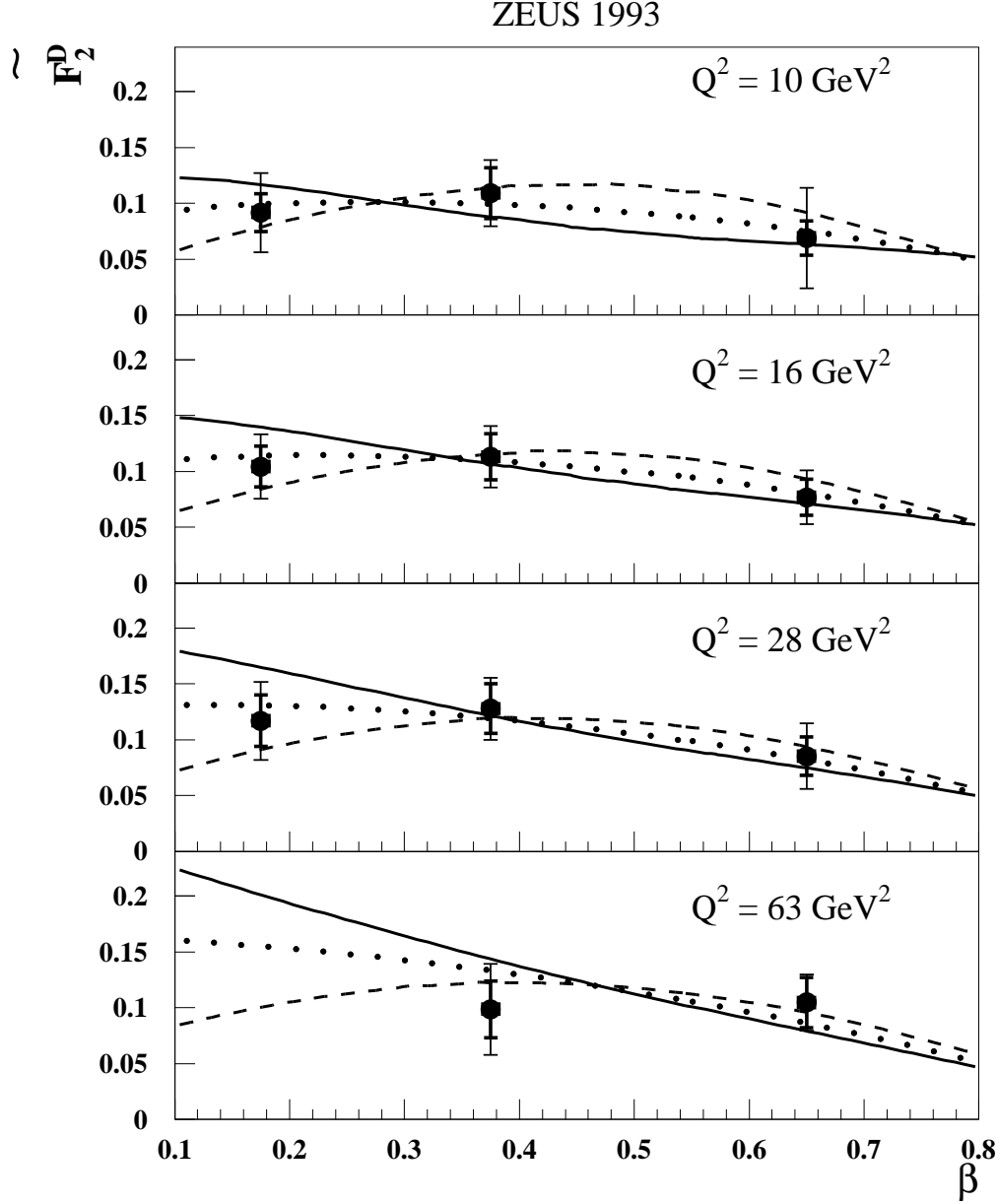


Figure 7: Measurements of $\tilde{F}_2^D(\beta, Q^2)$ in DIS [13] as a function of β for fixed values of Q^2 compared to the results of the QCD fits: “hard quark + hard gluon” (solid lines), “hard quark + leading gluon” (dashed lines) and “hard quark + (hard & leading) gluon” (dotted lines) parametrisations. The measurements contain an estimated $(31 \pm 13)\%$ contribution from double dissociation and the results of the QCD fits have been scaled up to take into account this contribution.

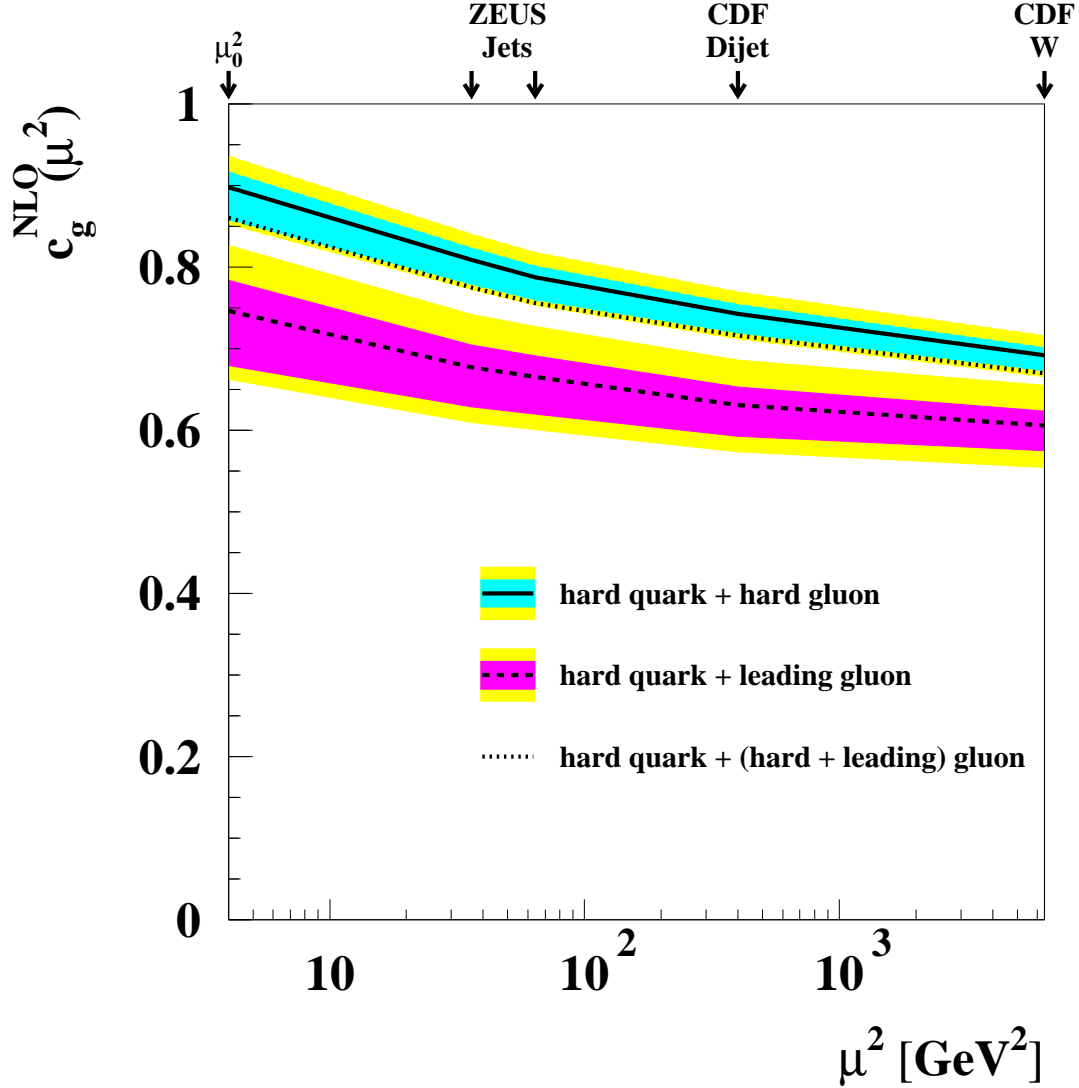


Figure 8: The values of $c_g^{NLO}(\mu^2)$ as a function of μ^2 for each of the QCD fits described in the text. For the “hard quark + hard gluon” (upper band) and “hard quark + leading gluon” (lower band) parametrisations, the central values (indicated by the lines), the statistical and systematic uncertainties –not associated with the absolute energy scale of the jets– added in quadrature (light-shaded bands) and the uncertainty due to the absolute energy scale of the jets (dark-shaded bands) are shown. The theoretical uncertainties are included in the light-shaded bands and discussed in the text. For the “hard quark + (hard & leading) gluon” parametrisation, only the central values are shown (dotted line). The μ^2 values at which $c_g^{NLO}(\mu^2)$ has been computed are indicated by the arrows.